Chemical and Spatial Differentiation of Syringyl and Guaiacyl Lignins in Poplar Wood via Time-of-Flight Secondary Ion Mass Spectrometry

ARTICLE *in* ANALYTICAL CHEMISTRY · AUGUST 2011

Impact Factor: 5.64 · DOI: 10.1021/ac200903y · Source: PubMed

5 AUTHORS, INCLUDING:

Chuanzhen Zhou
North Carolina State University
25 PUBLICATIONS **309** CITATIONS
SEE PROFILE

Quanzi Li
Chinese Academy of Forestry
36 PUBLICATIONS **649** CITATIONS
SEE PROFILE

Lucian Amerigo Lucia
North Carolina State University
238 PUBLICATIONS **3,051** CITATIONS
SEE PROFILE

analytical chemistry

ARTICLE

pubs.acs.org/ac

Chemical and Spatial Differentiation of Syringyl and Guaiacyl Lignins in Poplar Wood via Time-of-Flight Secondary Ion Mass Spectrometry

Chuanzhen Zhou,[†] Quanzi Li,[‡] Vincent L. Chiang,[‡] Lucian A. Lucia,[§] and Dieter P. Griffis*[,†,∥]

[†]Analytical Instrumentation Facility, Campus Box 7531, Room 318 MRC, 2410 Campus Shore Drive, [‡]Forest Biotechnology Group, Department of Forestry and Environmental Resources, [§]Department of Forest Biomaterials, Campus Box 8005, and [∥]Department of Materials Science and Engineering, Campus Box 7907, North Carolina State University, Raleigh, North Carolina 27695, United States

ABSTRACT: As a major component in plant cell walls, lignin is an important factor in numerous industrial processes, especially in wood saccharification and fermentation to biofuels. The ability to chemically differentiate and spatially locate lignins in wood cell structures provides an important contribution to the effort to improve these processes. The spatial distribution of the syringyl (S) and guaiacyl (G) lignins, both over larger regions and within a single cell wall, on poplar (*Populus trichocarpa*) wood cross sections was determined via time-of-flight secondary ion mass spectrometry (ToF-SIMS). This is the first time that direct chemically specific mass spectrometric mapping has been employed to elucidate the spatial distribution of S and G lignins. In agreement with results obtained by UV microscopy, ToF-SIMS images clearly show that the guaiacyl lignin is predominantly located in the vessel cell walls of poplar wood while syringyl lignin is mainly located in the fiber cell walls. The G/S ratio in vessel cell walls was determined to be approximately twice that found in fiber cell walls. A combination of Bi ToF-SIMS spectral image acquisition and C_{60} sputtering provided the ability to attain the combination of spatial resolution and signal-to-noise necessary to determine the distribution of S and G lignins in a single cell wall. By this technique, it was possible to demonstrate that more guaiacyl lignin is located in the middle lamella layer and more syringyl lignin is located in the inner cell wall area.

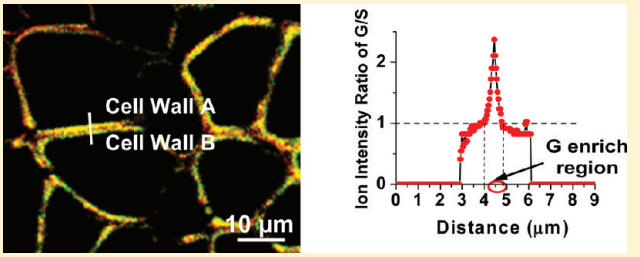

INTRODUCTION

Lignin biopolymer is a major component of the cell walls of all vascular plants. It primarily serves to bond together cellulosic materials in cell walls while facilitating water transport and providing a physical barrier to resist microbial activities. All lignins are based on one or more covalently coupled combinations of three lignin precursors: *p*-hydroxycinnamyl alcohol, coniferyl alcohol, and sinapyl alcohol, which give rise to the building blocks of *p*-hydroxyphenyl (H), guaiacyl (G), and syringyl (S) subunits (Figure 1).

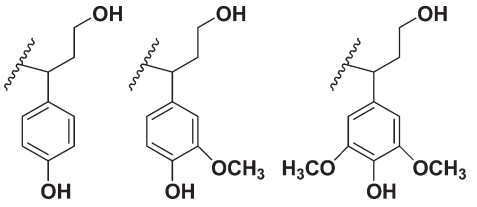

Figure 1. Chemical structure of the precursors of *p*-hydroxyphenyl (H), guaiacyl (G), and syringyl (S) subunits.

Efforts to use wood as a biomass feed stock for biofuels are accelerating, and the content and distribution of lignins in wood is a critical factor in industrial processes for its conversion into biofuels.[1−4] Efforts to develop and improve these processes will greatly benefit from a minimally destructive analytical technique with the spatial resolution and chemical specificity to map lignin distributions. Previous work that used UV microscopy and autoradiography showed that G predominates in the vessel elements of angiosperms and is deposited in the middle lamella, whereas the fiber and ray parenchyma secondary walls are rich in S.[5−9] Other techniques currently in use to interrogate the structural and chemical composition of wood include near-infrared (NIR), mid-infrared, Raman spectroscopy,[10] and high-resolution solution-state nuclear magnetic resonance.[11] However, these techniques lack the ability to simultaneously provide the unambiguous chemical specificity and spatial resolution required to determine the spatial distribution of G and S lignin in wood. Time-of-flight secondary ion mass spectrometry (ToF-SIMS) has tremendous potential to provide the ability to both chemically identify and determine the spatial distribution of S and G lignin via direct mass spectrometric measurement. In previous studies, ToF-SIMS has been applied to the examination of metal localization in oxidized pulps,[12] characterization of lignin and polysaccharides in wood[13] and the chemical structure of lignin.[14] However, the ability to obtain the spatial resolution required for characterization of G and S lignin distribution in wood has been hampered by two factors: (1) artifacts resulting from the microtome sample preparation process[13], which can smear the surface

Received: April 8, 2011
Accepted: August 18, 2011

   dx.doi.org/10.1021/ac200903y | *Anal. Chem.* XXXX, XXX, 000–000

and leave debris, thus reducing spatial resolution and masking surface chemistry; and (2) the finite lifetime of lignin moieties due to their destruction by the high-energy ion bombardment during ToF-SIMS spectral image data acquisition, which limits the number of obtainable secondary ions characteristic of the lignins and thus limits the signal-to-noise ratio.

Recently C_{60} sputtering has been shown, in some cases,[15−18] to provide the ability to remove organic surface material with significantly reduced destruction of surface chemistry compared with that resulting from Bi bombardment. In this study, a protocol based on alternating C_{60} sputtering and Bi_3^+ spectral imaging is employed both to remove surface contamination and debris resulting from microtome sample preparation and also to remove material damaged by Bi_3^+ SIMS primary ion bombardment with limited destruction of lignin chemistry. This protocol provides the combination of high spatial resolution and high signal-to-noise ratio required to obtain spatially resolved direct mass spectrometric measurement of S and G lignin within a cell wall.

EXPERIMENTAL SECTION

Preparation of Poplar Stem Cross Sections. Segments of *Populus trichocarpa* (Nisqually-1) stem internodes (7 and 8) were fixed in FAA solution containing (v/v) 50% ethanol, 10% glacial acetic acid, and 10% formaldehyde (37% solution) overnight at room temperature. These segments were then dehydrated through an ethanol series, followed by incubation in wax (Paraplast Plus tissue embedding medium) for 4 days with replacements of fresh wax twice per day. Sections (12 μm thick) were microtomed from the wax-embedded segments, which were then mounted on slides at 42 °C overnight. Segments were incubated in wax to preserve the cell structure to the maximum possible extent and to obtain the flattest possible sectioned surface for better ToF-SIMS secondary ion extraction. Prior to ToF-SIMS analysis, sections were dewaxed twice in xylene for 10 min and dried at room temperature.

Time-of-Flight Secondary Ion Mass Spectrometric Analysis. ToF-SIMS is a highly sensitive surface analytical technique for acquisition of elemental and molecular information from the surface (top 1−2 nm) of a material, with both high spatial and mass resolution. For ToF-SIMS spectrum and image acquisition, a finely focused, pulsed primary ion beam is rastered across the surface of the sample and the secondary ions emitted at each irradiated point or pixel are extracted into a time-of-flight mass spectrometer, mass-filtered, and counted. In this way, an image with submicrometer (<0.3 μm) spatial resolution can be acquired with a full mass spectrum for each pixel (spectrum image). ToF-SIMS analyses in this study were conducted on a ToF-SIMS V (ION TOF, Inc. Chestnut Ridge, NY) instrument equipped with a Bi_n^{m+} (n = 1−5, m = 1, 2) liquid metal ion gun and a C_{60} ion gun. The instrument vacuum system consists of a load lock for rapid sample loading and an analysis chamber separated by the gate valve. The analysis chamber pressure is maintained below 5.0×10^{-9} mbar to avoid contamination of the surfaces to be analyzed.

High mass resolution spectra were acquired by use of a 25 keV Bi^+ liquid metal ion source at a current of 0.4 pA, with a pulse width of 1.3 ns. Secondary ions were extracted into a ToF mass spectrometer with 10 keV post acceleration to improve detection sensitivity. The combination of primary ion pulse width used and the ToF analyzer tuning provides a mass resolution of approximately 3000−4000 m/Δm at m/z 29 ($C_2H_5^+$). Spectrum images (256 × 256 pixels) were acquired by use of a 25 keV Bi_3^+ liquid metal ion source at a current of 0.07 pA, with a pulse width of 100 ns. An electron flood gun (300 V) was used to prevent charge buildup on the insulting sample surfaces. The total accumulated primary ion dose for the spectra acquisition and image acquisition of the 500 μm × 500 μm areas was less than 1×10^{13} ions/cm^2, a total ion dose that is within the static SIMS regime.[19] The total ion dose for the image of 100 μm × 100 μm area (1500 scan, 1 shot/pixel) was 4×10^{13} ions/cm^2, which exceeds the static SIMS regime. Conditions for the cyclic damage removal, improved signal-to-noise experiment using the C_{60}^+ and Bi_3^+ primary ion beams is as follows: a 300 μm × 300 μm area of the surface of the wood cross-section was sputtered for 10 s with 0.25 nA C_{60}^+ ion beam. A ToF-SIMS image of a 100 μm × 100 μm area was acquired with Bi_3^+ at 50 pulses/pixel, and this sequence was then repeated 34 times.

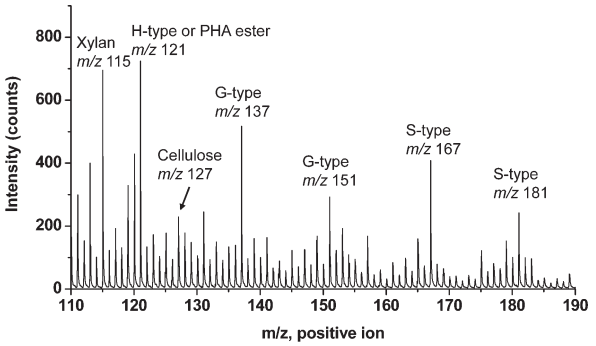

Figure 2. Positive-ion ToF-SIMS spectra obtained from the surface of a cross section of *P. trichocarpa* wood xylem showing the characteristic ions for carbohydrates and for guaiacyl and syringyl lignins. Exact masses of the labeled peaks are as follows. Carbohydrates: $[C_5H_7O_3]^+$ = 115.0395 for xylan; $[C_6H_7O_3]^+$ = 127.0395 for cellulose. Lignins: $[C_7H_5O_2]^+$ = 121.0289 for H; $[C_8H_9O_2]^+$ = 137.0603 and $[C_8H_7O_3]^+$ = 151.0395 for G; $[C_9H_{11}O_3]^+$ = 167.0708 and $[C_9H_9O_4]^+$ = 181.0501 for S.

RESULTS

High Mass Resolution Spectra of Poplar Wood Cross-Section. Figure 2 shows the high mass resolution positive-ion ToF-SIMS spectrum acquired for the *P. trichocarpa* wood cross-section surface after paraffin removal. In addition to low mass metal (Na^+, Mg^+, Ca^+) and other secondary ions, the spectrum of the wood cross-section exhibits a number of secondary ions that are characteristic of carbohydrates (m/z 115 $C_5H_7O_3^+$; m/z 127 $C_6H_7O_3^+$)[20] and lignin characteristic ions including hydroxyphenyl (H-type, m/z 121 $C_7H_5O_2^+$),[21,22] guaiacyl (G-type),[14,22,23] and syringyl (S-type).[14,22,23] It is noted that the ion intensity at m/z 121 is quite high for H-type lignin. The high ion intensity at m/z 121 is probably due to *p*-hydroxybenzoic acid (PHA) esterified to lignins in the cell wall in poplar wood, which has the same fragment ion as the H-type lignin.[24,25] The characteristic ions originating from guaiacyl are m/z 137 ($C_8H_9O_2^+$) and m/z 151-($C_8H_7O_3^+$) while the characteristic ions originating from syringyl are m/z 167 ($C_9H_{11}O_3^+$) and m/z 181 ($C_9H_9O_4^+$). Molecular structures of the fragment ions for guaiacyl and syringyl characteristic ions are shown in Figure 3.

High Spatial Resolution Imaging of Poplar Wood Cross Sections: Distribution of Guaiacyl and Syringyl Lignins over Larger Cell Wall Regions. Poplar wood cross sections were

dx.doi.org/10.1021/ac200903y |*Anal. Chem.* XXXX, XXX, 000–000

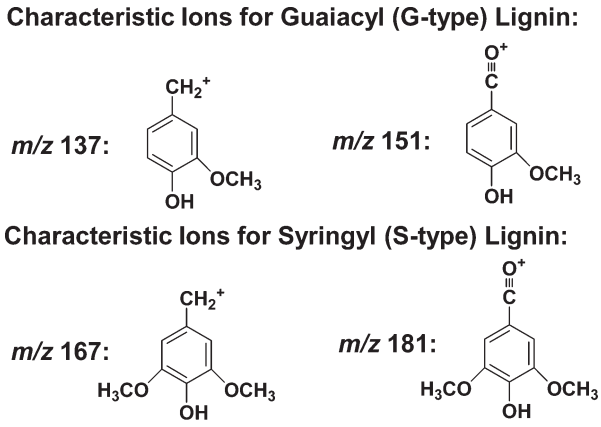

Figure 3. Chemical structure of the characteristic fragment ions attributed to guaiacyl and syringyl lignins.

prepared by microtoming chemically fixed, paraffin-embedded stem sections onto a glass slide. Low-resolution (limited by the ToF-SIMS V camera/microscope optics) macroscopic and microscopic optical images showing the area of the sample to be analyzed are presented in Figure 4a,b. Note that while the optical resolution of these images is rather low, the images are only intended for (and their resolution is sufficient for) initially locating the stem section on the sample holder and then locating the area of the section to be analyzed by ToF-SIMS. It can also be seen from these images that the microtomed cross-section is flat and free of large debris.

A 256 × 256 pixel ToF-SIMS image was acquired over the 500 μm × 500 μm area shown in Figure 4b, and the mass spectra acquired for each pixel were stored for retrospective data analysis. The integrated intensities of the G fragment ion peaks at m/z 137 and 151 at each pixel location were summed to produce an image displaying the relative abundance of G across the area analyzed (Figure 4c) to a color scale from black (lowest intensity) to bright red (highest intensity). This process was then repeated for the S fragment ion intensities at m/z 167 and 181 to produce and store a similar image showing the relative abundance of S (Figure 4d) to a color scale from black to green. These two images were then combined to show the relative distributions of G (red) and S (green) over the area of the stem section analyzed. With this color mapping, areas rich in G are red, areas rich in S are green, and areas containing a mixture of G and S are yellow (combination of red and green). The combined ToF-SIMS image (Figure 4e) clearly shows the spatial distribution of G and S lignins over the 500 μm × 500 μm region of the stem analyzed. G (in red) is predominantly located in the vessel cell areas, whereas S (in green) is predominantly located in the fiber cell areas. To our knowledge, this is the first time that the spatial distribution of G and S has been directly visualized via mass spectrometric chemical composition mapping. It is noted that the lower right area shows very low ion intensities of G and S lignin. This region is close to cambium, where the cells are undergoing secondary cell wall thickening. Compared to the cells in the upper left region, the cells in this region have very low lignin content due to the thin secondary cell walls in this region.

While the data presented above provide a visual representation of the relative abundance of G and S across the area analyzed, further analysis was required to obtain a semiquantitative comparison of the relative abundance of G and S in the vessel cell wall

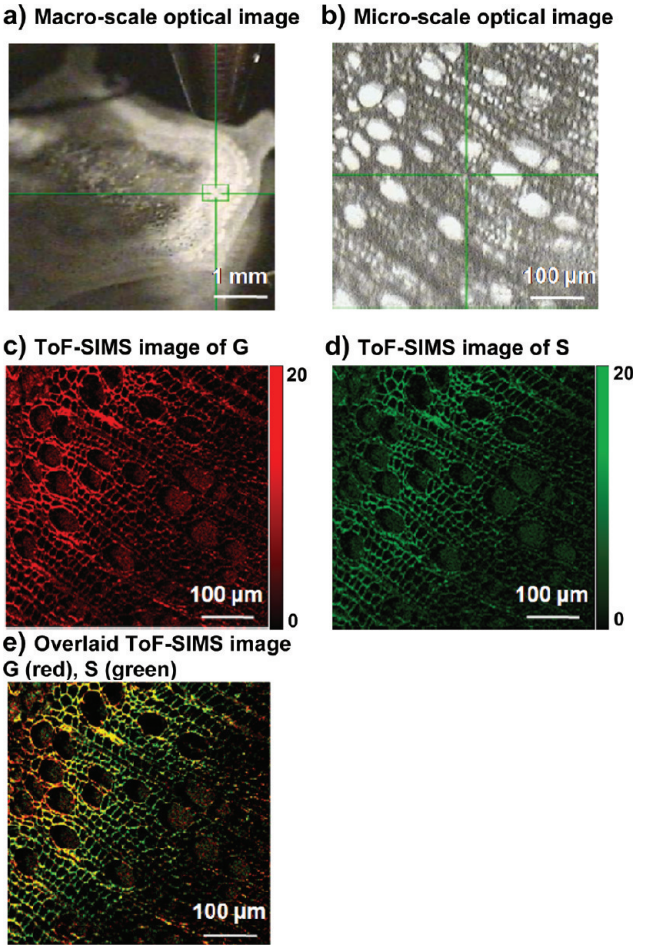

Figure 4. (a) Macroscale and (b) microscale optical images captured by the respective sample viewing cameras of ToF-SIMS. (c–e) ToF-SIMS images of (c) guaiacyl (G), (d) syringyl (S), and (e) overlaid images of G (in red) and S (in green) of the wood cross-section.

versus the fiber cell wall areas. To semiquantitatively compare the relative abundances of G and S in vessel cell walls versus fiber cell walls, regions of the microtomed stem cross section (denoted as regions of interest or ROI's; shown in Figure 5a) were carefully selected to contain vessel cell walls away from fiber cell walls (ROI 1), vessel cell walls closer to fiber cell walls (ROI 2), and fiber cell walls (ROI 3). The mass range containing the G and S characteristic secondary ions of the ToF-SIMS spectra obtained from all pixels within these respective ROI's were then summed and the resulting mass spectra of these ROI's were normalized to m/z 181and overlaid (Figure 5b). Comparison of the respective heights of the m/z 137 and 151 peak intensities for the three ROI's indicates that more G lignin (a higher G/S ratio) is contained in vessel cell walls (ROI 1 and 2) than in fiber cell walls (ROI 3). This observation was confirmed by a detailed analysis of three additional areas for each of the three ROI types described above (additional data not shown). The combined results of these analyses are shown in Figure 5c. The G/S ratio is 2.1 for the vessel cells farthest from the fiber cells (ROI 1), 1.5 for the vessel cell walls closer to the fiber cells (ROI 2), and 0.9 for the fiber cell walls (ROI 3), within 10% standard deviation.

Distribution of Guaiacyl and Syringyl Lignin in the Cell Wall of a Single Vessel or Fiber Cell. While the ToF-SIMS data presented above clearly show that the G/S ratio in vessel cell

dx.doi.org/10.1021/ac200903y |*Anal. Chem.* XXXX, XXX, 000–000

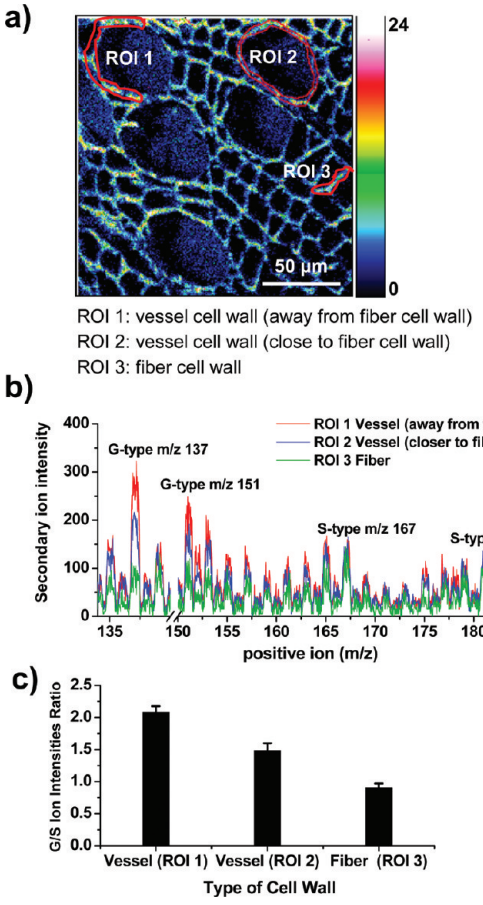

Figure 5. (a) ToF-SIMS image (180 μm × 180 μm, 256 × 256 pixels) of guaiacyl lignin showing the regions of interest (ROI's) analyzed. ROI 1 contains vessel cell walls away from the fiber cell walls, ROI 2 contains vessel cell walls closer to fiber cell walls, and ROI 3 contains fiber cell walls. (b) Overlaid ToF-SIMS spectra reconstructed from ROI 1, ROI 2, and ROI 3. The spectra are normalized at m/z 181, which is one of the characteristic ions of syringyl lignin. (c) Lignin G/S ratios for the ROIs.

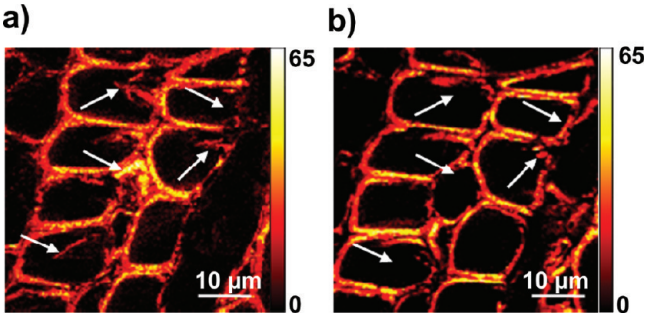

Figure 6. ToF-SIMS images of a selected area for syringyl lignin from 100 μm × 100 μm, 256 × 256 pixel images. Image a was acquired only with 1500 scans of Bi_3^+, and image b was acquired with C_{60}^+ sputtering for 40 s followed by 1500 scans of Bi_3^+. S images are the summation of characteristic ions at m/z 167 and 181.

walls is approximately twice that present in the fiber cell walls, the spatial resolution of the images (e.g., Figure 5a) is not sufficient to determine the distribution of G and S lignins within the cell wall of a single cell. The lack of spatial resolution in Figure 5a is not the result of a lack of resolution of the Bi_3^+ beam utilized for data acquisition. Whenever the ToF-SIMS is aligned for high spatial resolution imaging, a resolution test is performed to demonstrate that the Bi_3^+ beam is aligned to provide a ≤300 nm beam spot size. With this knowledge and in view of the low number of G and S secondary ion counts per pixels, it was deemed likely that the lack of spatial resolution resulted from a combination of sample surface smearing and debris resulting from the microtome sample preparation and the inability to acquire sufficient quantities of G and S secondary ions (secondary ion counts) as a result of the destruction of the G and S molecular structure by Bi_3^+ bombardment. To recover the lost spatial resolution and to improve signal-to-noise, a data acquisition/surface cleaning and damage removal protocol was devised that employs a combination of Bi_3^+ data acquisition followed by C_{60}^+ ion beam sputtering to remove the surface layer damaged by Bi_3^+ bombardment.

The ability of C_{60} sputtering to clean the surface was demonstrated by a set of experiments performed as follows. A 100 μm × 100 μm area, 256 × 256 pixel ToF-SIMS image was acquired on a wood cross section with one Bi_3^+ primary ion pulse per pixel for 1500 scans. The resulting image of a selected area for syringyl (sum of m/z 167 and 181) is presented in Figure 6a. Another 100 μm × 100 μm area, 256 × 256 pixel image was acquired at, as nearly as possible, an identical position on a second wood cross section employing 40 s of C_{60} sputtering to remove surface smearing and debris followed by 1500 scans of one Bi_3^+ primary ion pulse per pixel. The image of syringyl from this acquisition is presented in Figure 6b. It can be clearly seen that, with C_{60} sputtering to remove microtome-induced smearing, the areas indicated by the white arrows in Figure 6a were removed with the result that the cell wall edges are sharper and cleaner and the overall spatial resolution of the image is greatly improved. However, examination of the summed spectra from the images shown in Figure 6 showed that they were almost identical in terms of both secondary ion species and secondary ion intensities, suggesting that while surface cleaning can improve spatial resolution, the signal-to-noise ratio was still not sufficient to determine the spatial distribution of G and S lignin in a single cell wall. Therefore, additional effort is needed to address the issue of lignin fragment destruction resulting from Bi_3^+ spectral image data acquisition.

Normalized ion intensity profiles of syringyl (m/z 181) obtained from the summation images acquired only with Bi_3^+ but with no surface cleaning (Figure 6a), images acquired with Bi_3^+ after C_{60} sputtering (Figure 6b) and images acquired by use of a cyclic C_{60} sputtering damage removal protocol (Figure 8b) are presented for comparison in Figure 7. This latter image (Figure 8b) was acquired by utilization of the Bi_3^+ data acquisition/C_{60}^+ cyclic cleaning and damage removal protocol: the surface of the wood cross-section was sputtered for 10 s with 0.25 nA C_{60}^+ ion beam, a ToF-SIMS image was acquired with Bi_3^+ at 50 pulses/pixel, and this sequence was then repeated. To allow direct comparison of the respective decreases of lignin ion intensity obtained via the three data acquisition approaches, the initial secondary ion intensity at m/z 181 for all sets of data is normalized to 1. While the lignin ion intensity decreases in all cases, the extent of decrease in lignin ion intensity is significantly less for the image acquired via the C_{60} cyclic damage removal protocol (55% of initial ion intensity) than the images acquired without the use of C_{60} sputtering to remove Bi_3^+ chemical damage (40% of initial ion intensity). Although C_{60} sputtering does not retain or restore the initial m/z 181 intensity, it does help to significantly improve

dx.doi.org/10.1021/ac200903y |*Anal. Chem.* XXXX, XXX, 000–000

the signal-to-noise ratio by allowing at least partial recovery of the m/z 181 secondary ion intensity. Further studies are required to determine the optimized combination of C_{60} sputtering versus the number of Bi_3^+ pulses/pixel needed to produce maximum signal recovery.

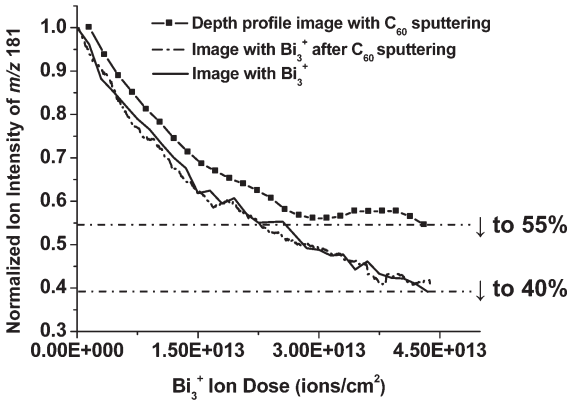

Figure 7. Ion intensity profile of m/z 181 for the images acquired only with Bi_3^+ (shown in Figure 6a), with Bi_3^+ after C_{60} surface cleaning (shown in Figure 6b) and by use of the C_{60} cyclic damage removal protocol (shown in Figure 8b). The initial ion intensity is normalized to 1 for a direct comparison.

It was determined from examination of the individual images obtained from the 34 sputtering/acquisition cycles that images 1−4 were noisy, perhaps due to smearing of the wood surface during microtoming, so these images were discarded and the remaining 30 images were summed to produce the image presented in Figure 8a. It is readily apparent that the spatial distributions of the G and S lignins in Figure 8a are distinguishable in individual cell walls. It can be seen that more G lignin (red) is located in the outer cell wall layers, which are between the two adjacent cell walls (probably the middle lamella layer) and more S lignin (green) is located in the inner cell wall layer (the secondary cell wall layer). The lignin distribution across the cell walls is most apparent in the areas delineated by the red boxes in the zoomed in image of Figure 8a. Figure 8b is an SEM image of a fiber cell wall acquired from a similar wood segment sample prior to ToF-SIMS analysis to illustrate the structure of the middle lamellar layer and the secondary cell wall layer. It can be seen in Figure 8 that there are voids and small gaps in certain areas at

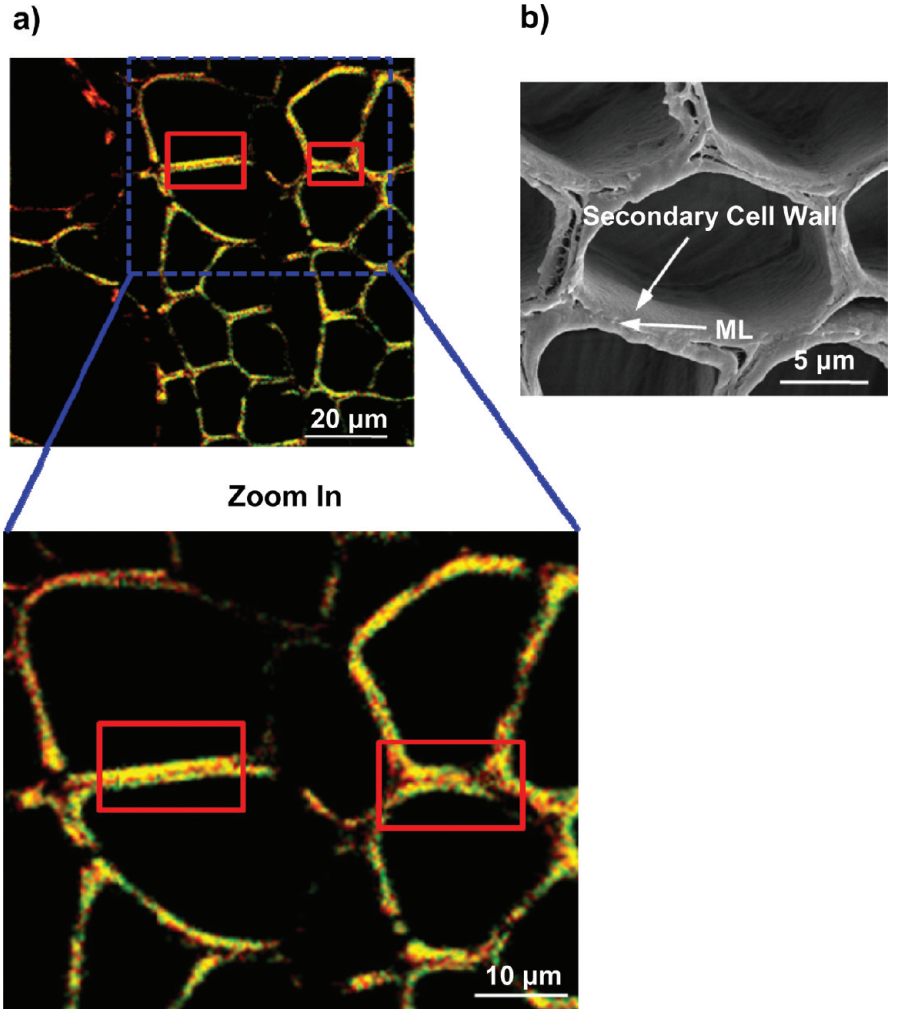

Figure 8. (a) ToF-SIMS image of wood cell cross sections (100 μm × 100 μm, 256 × 256 pixels) in which guaiacyl (G, in red) and syringyl (S, in green) lignin images have been overlaid. The ToF-SIMS image was acquired via the C_{60}^+ sputtering damage removal protocol (details given above). G images used in the overlays are the summation of characteristic ions at m/z 137 and 151, and S images are the summation of characteristic ions at m/z 167 and 181. The SEM image of a fiber cell wall in panel b is acquired before ToF-SIMS analysis and is included to illustrate the structure of the middle lamellar layer and the secondary cell wall layer. See the description on SEM preparation in Li et al.[26]

dx.doi.org/10.1021/ac200903y |*Anal. Chem.* XXXX, XXX, 000–000

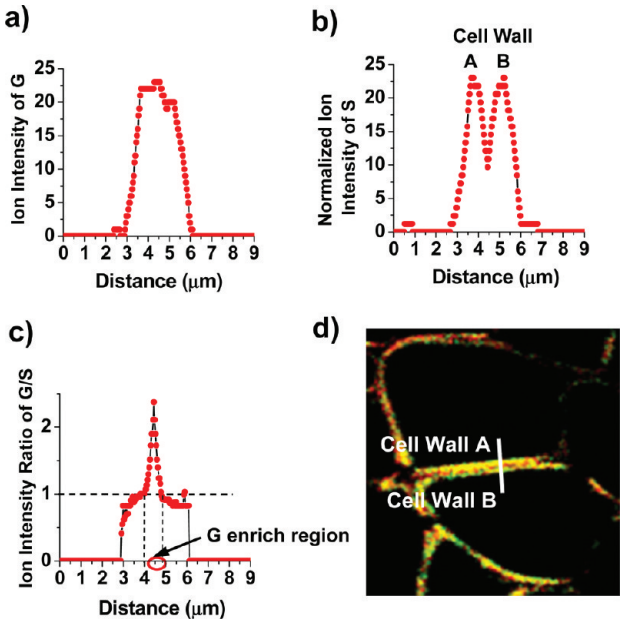

Figure 9. Line scan intensity profiles of (a) guaiacyl, (b) syringyl, and (c) the G/S ratio across two adjoining fiber cell walls. The G and S overlaid ToF-SIMS image showing the two adjoining cell walls (A and B) and the portion of the cell wall from which the line scans were taken (white line) is shown in panel d.

corners and between cell walls, which result in low secondary ion intensities. It is suspected that these voids may result from the sample preparation and microtome sectioning process.

To further characterize the spatial distributions of the guaiacyl and syringyl lignins across an individual cell wall, line intensity profiles (see white line in Figure 9d) of the G and S distributions and of the G/S ratio across two adjoining cell walls are presented in Figure 9. The line intensity profiles of G lignin in Figure 9a and S lignin in Figure 9b clearly show differences in the distributions of G and S lignins across the two adjoining, approximately 1.5 μm thick fiber cell walls. G type lignin is greater in the region where the walls of two fiber cells are touching, in comparison to the much lower S type lignin in the same region. The ratio of the G and S data shown in panels a and b is plotted in Figure 9c to further illustrate the predominance of guaiacyl lignin in the outer portion of the two adjacent fiber cell walls. A much higher G/S ratio is observed between the two cell walls from ~4 to 4.8 μm in Figure 9c.

DISCUSSION

In previous work, UV microscopy has been used to map the spatial distribution of guaiacyl and syringyl lignins in wood cross sections.[5,8,9] In this study, these findings have now been confirmed and expanded via direct mass spectrometric measurement of G and S lignin in *P. trichocarpa* wood. It is interesting to note that the difference in the G/S ratio observed in the vessel cell walls versus the fiber cell walls for *P. trichocarpa* wood by ToF-SIMS is approximately a factor of 2, consistent with the UV microscopic study results.[9] The ability of the ToF-SIMS protocol utilized in this work to directly probe the spatial distribution of lignin in wood via mass spectrometric chemical mapping was made possible by the use of a cyclic cleaning and damage removal protocol employing C_{60}^+ ion beam sputtering. C_{60} was used to first sputter-clean the surface to remove microtome sample preparation damage and then, in subsequent data acquisition cycles, to sputter away at least a portion of the surface layer damaged by the Bi ion beam during image acquisition. This combination of improvements was sufficient to expose relatively undamaged lignin molecules below the Bi-induced damaged layer, making available sufficient numbers of secondary ions characteristic of G and S lignins to provide a meaningful improvement in signal-to-noise ratio. This combination of damage removal and signal-to-noise ratio improvement makes it possible for the first time to resolve the spatial distribution of guaiacyl and syringyl lignin in a single cell wall by direct mass spectrometric chemical mapping, allowing the unambiguous determination that more guaiacyl lignin is present in the outer cell wall region corresponding to the middle lamella layer.

CONCLUSION

For the first time, direct mass spectrometric chemical mapping was used to elucidate the spatial distribution of the guaiacyl and syringyl lignins, both locally and over a larger region on *P. trichocarpa* wood cross sections. ToF-SIMS images clearly demonstrate that the lignin located in the vessel cell wall of poplar wood is mainly guaiacyl type while the fiber cell wall lignin is predominantly syringyl type. The difference in the G/S ratio observed in the vessel cell walls versus the fiber cell walls by ToF-SIMS is approximately a factor of 2, consistent to that obtained from UV microscopy, suggesting that it may be possible to use ToF-SIMS for relative quantitative analysis of G and S lignins in wood. The capability of C_{60}^+ ion source to remove both surface smearing and damage resulting from the microtome process. as well as to at least partially remove Bi-induced damage, provided the ability to directly determine G and S lignin distribution within a single cell wall: that is, guaiacyl lignin is preferentially located in the middle lamella layer and syringyl lignin is preferentially located in the inner cell wall area. Further study is needed to optimize the C_{60} cyclic damage removal process to explore the possibility of further improvement in ToF-SIMS direct chemical mapping of lignins in wood.

AUTHOR INFORMATION

Corresponding Author

*E-mail: dgriffis@ncsu.edu. Phone: 919-515-2128. Fax: 919-515-6965.

ACKNOWLEDGMENT

This research was made possible in part with support from the William R. Kenan, Jr. Institute for Engineering, Technology & Science at NC State University and by the North Carolina State University Analytical Instrumentation Facility.

REFERENCES

(1) Shi, R.; Sun, Y.-H.; Li, Q.; Heber, S.; Sederoff, R.; Chiang, V. L. *Plant Cell Physiol.* **2010**, *51*, 144–163.
(2) Sarkanen, K. V. *Science* **1976**, *191*, 773–776.
(3) Ragauskas, A.; Williams, C.; Davison, B.; Britovsek, G.; Cairney, J.; Eckert, C. A. *Science* **2006**, *311*, 484–489.
(4) Chen, F.; Dixon, R. *Nat. Biotechnol.* **2007**, *25*, 759–761.
(5) Fergus, B. J.; Foring, D. A. I. *Holzforschung* **1970**, *24*, 113–117.
(6) Saleh, T. M.; Leney, L.; Sarkanen, K. V. *Holzforschung* **1967**, *21*, 116–120.

(7) Musha, Y.; Goring, D. A. I. *Can. J. For. Res.* **1975**, *5*, 259–268.
(8) Fergus, B. J.; Goring, D. A. I. *Holzforschung* **1970**, *24*, 118–124.
(9) Musha, Y.; Goring, D. A. I. *Wood Sci. Technol.* **1975**, *9*, 45–58.
(10) Schmidt, M.; Schwartzberg, A. M.; Perera, P. N.; Weber-Bargioni, A.; Carroll, A.; Sarkar, P.; Bosneaga, E.; Urban, J. J.; Song, J.; Balakshin, M. Y.; Capanema, E. A.; Auer, M.; Adams, P. D.; Chiang, V. L.; Schuck, P. J. *Planta* **2009**, *230*, 589–597.
(11) Yelle, D. J.; Ralph, J.; Frihart, C. R. *Magn. Reson. Chem.* **2008**, *46*, 508–517.
(12) Mancosky, D. G.; Lucia, L. A. *Pure Appl. Chem.* **2001**, *73*, 2047–2058.
(13) Tokareva, E. N.; Fardim, P.; Pranovich, A. V.; Fagerholm, H.-P.; Daniel, G.; Holmbom, B. *Appl. Surf. Sci.* **2007**, *253*, 7569–7277.
(14) Saito, K.; Kato, T.; Tsuji, Y.; Fukushima, K. *Biomacromolecules* **2005**, *6*, 678–683.
(15) Wucher, A.; Winograd, N. *Anal. Bioanal. Chem.* **2010**, *396*, 105–114.
(16) Weibel, D. E.; Lockyer, N.; Vickerman, J. C. *Appl. Surf. Sci.* **2004**, *231−232*, 146–152.
(17) Nieuwjaer, N.; Poleunis, C.; Delcorte, A.; Bertrand, P. *Surf. Interface Anal.* **2007**, *41*, 6–10.
(18) Fisher, G. L.; Dickinson, M.; Bryan, S. R.; Moulder, J. *Appl. Surf. Sci.* **2008**, *255*, 819–823.
(19) Benninghoven, A. *Surf. Sci.* **1973**, *35*, 427–437.
(20) Fardim, P.; Durán, N. *Colloids Surf.,A* **2003**, *223*, 263–276.
(21) Kleen, M. *Holzforschung* **2005**, *59*, 481–487.
(22) Saito, K.; Kato, T.; Takamori, H.; Kishimoto, T.; Yamamoto, A.; Fukushima, K. *Appl. Surf. Sci.* **2006**, *252*, 6734–6737.
(23) Saito, K.; Kato, T.; Takamori, H.; Kishimoto, T.; Fukushima, K. *Biomacromolecules* **2005**, *6*, 2688–2696.
(24) Sun, R.; F., S. X.; Wang, S. Q.; Zhu, W.; Wang, X. Y. *Ind. Crop Prod.* **2002**, *15*, 179–188.
(25) Smith, D. C. *J. Chem. Soc.* **1955**, 2347–2351.
(26) Li, Q.; Min, D.; Wang, J. P.; Peszlen, I.; Horvath, L.; Horvath, B.; Nishimura, Y.; Jameel, H.; Chang, H.-M.; Chiang, V. L. *Tree Physiol.* **2011**, *31*, 226–236.